Magnetic resonance study of the Fe^+(I) center in $SrCl_2$ single crystals

H. Vrielinck, F. Callens, and P. Matthys
Department of Solid State Sciences, Ghent University, Krijgslaan 281-S1, B-9000 Ghent, Belgium

S. V. Nistor and D. Ghica
National Institute of Material Physics, POB MG-7 Magurele, 76900 Bucharest, Romania

D. Schoemaker
Physics Department, University of Antwerp (UIA), Universiteitsplein 1, B-2610 Antwerpen (Wilrijk), Belgium
(Received 18 December 2000; published 11 June 2001)

An Fe^+-type center with axial ⟨001⟩ symmetry has been studied by electron nuclear double resonance (ENDOR) in the microwave *X* and *Q* bands. The Fe^+(I) center is produced only after irradiation with x or γ rays at 80 K of $SrCl_2$:Fe^{2+} crystals grown in a Cl_2 atmosphere. It has a $3d^7\ {}^4F\Gamma_8$ ground state with spin $S=\frac{3}{2}$. As shown by the correlated analysis of the ENDOR data and electron paramagnetic resonance superhyperfine structure, the Fe^+ ion is situated in the center of a tetragonally compressed cube of eight nearest Cl^- ions. The simplest model of the Fe^+(I) center, compatible with the magnetic resonance results, consists of an interstitial Fe^+ ion with two substitutional monovalent cations, very likely K^+ ions, in two opposite nearest-neighbor Sr^{2+} sites along the tetragonal axis of the center.

DOI: 10.1103/PhysRevB.64.024405 PACS number(s): 76.30.Fc, 76.70.Dx, 61.72.Ww

I. INTRODUCTION

Single crystals of $SrCl_2$ grown and doped with iron in a chlorine atmosphere (chlorinated) contain Fe^{2+} related electron and hole trapping centers, which have not been found in crystals grown by conventional procedures, i.e., in vacuum or an inert gas. The trapping of electrons/holes produced by subsequent short irradiation at low temperatures with ionizing radiation (high-energy electrons, x or γ rays) at such precursor Fe^{2+} centers results in corresponding paramagnetic Fe^+/Fe^{3+} centers, which can be easily observed and studied by electron paramagnetic resonance (EPR) and related techniques.

Applying such procedures resulted in the identification of a trapped hole Fe_t^{3+} center with local trigonal ⟨111⟩ symmetry[1] and of two trapped electron Fe^+(I) and Fe^+(II) centers, both with local tetragonal ⟨001⟩ symmetry.[2,3] These centers cannot be observed in irradiated $SrCl_2$:Fe crystals grown by conventional techniques, crystals in which only a trapped hole Fe_c^{3+} center with cubic symmetry has been reported.[4] It should be mentioned that the production of additional Fe^{2+} related electron/hole trapping precursor centers has been previously observed in chlorinated alkali chloride crystals as well.[5–7]

The mechanism responsible for the production of the precursor Fe^{2+} hole/electron trapping centers by chlorinating is not well understood yet, neither in alkali chlorides, nor in strontium chloride. In this respect, essential information may result from a detailed knowledge of the microstructure of the corresponding paramagnetic centers produced by irradiation at low temperature (below 100 K). Due to the absence of ionic movements at such temperatures, the paramagnetic centers produced by irradiation are expected to retain the structure of the precursor Fe^{2+} centers in the as-grown crystals.

Moreover, crystals with cubic fluorite structure, such as $SrCl_2$, provide the possibility to investigate the less known case of paramagnetic impurity ions in crystal fields with eightfold coordination, when impurity ions are substituted on cation sites. Indeed, compared to the large amount of data concerning the transition ions in sixfold and fourfold coordinated sites of the rock salt and diamond type lattices, respectively, the amount of published results on eightfold coordinated iron group transition ions is very limited.[8] Up to now, to our knowledge, there has been published only one paper reporting the observation of $Fe^+(3d^7)$ ions in a crystal lattice host (ThO_2) with fluorite structure.[9] In this case, the reduced ionic charge of the Fe^+ ion is compensated by the presence of a neighboring trivalent impurity ion, responsible for the local tetragonal distortion.

In order to understand the abovementioned aspects, we performed a combined *X* and *Q* band EPR and electron nuclear double resonance (ENDOR) study of the Fe^+(I) center, observed[2,3] in chlorinated $SrCl_2$:Fe^{2+} crystals after x ray irradiation at $T=80$ K. Our main effort has been directed towards determining its microstructure, nature, and localization of the neighboring ligands.

II. EXPERIMENTAL

A. Materials

$SrCl_2$ single crystals doped with Fe^{2+} were grown by the Bridgman technique in a Cl_2 atmosphere, as described in Ref. 1. It is estimated that due to segregation effects, less than 300 ppm from the 1000 ppm iron added to the melt enter the $SrCl_2$ lattice, mainly as Fe^{2+} ions. Before irradiation, the crystals were annealed to 700 K, in order to enhance the intensity of the resulting Fe^+(I) signal. The Fe^+(I) centers were produced by irradiation with x rays (*W* anticathode, 60 kV, 40 mA) at $T\approx 80$ K, for typically half an hour. Usually, after irradiation, in order to avoid the overlap with the

EPR lines from other paramagnetic centers, especially in the $g \approx 2$ region, the crystals were again annealed at 700 K. Without significantly changing the concentration of the Fe^+(I) centers, by this treatment all other Fe^+ and Fe^{3+} type of paramagnetic centers, simultaneously produced during irradiation, were bleached out. The crystals were cleaved with the long edge along crystal ⟨110⟩ directions, which allowed the angular dependence of the spectra to be recorded in a {110} plane. Typical sample sizes were $3\times3\times10\,mm^3$ in the *X* band and $1\times1\times5\,mm^3$ in the *Q* band. The samples were oriented in the magnetic field by inspection of the Fe^+(I)EPR spectrum (estimated accuracy 0.5°). An even higher accuracy (0.1°) could be obtained in as irradiated samples, with the aid of those transitions of the trigonal Fe_t^{3+} centers which are fourfold degenerate when the magnetic field lies along the ⟨001⟩ axis and twofold degenerate in the {110} planes.

B. Methods

The *X*-band EPR and ENDOR measurements were performed on a Bruker ESP300E spectrometer with a Bruker ESP353E ENDOR/TRIPLE extension [EN374 radio frequency (rf) amplifier and EN525 Schomandl synthesizer] equipped with an Oxford ESR10 flow cryostat. The *Q*-band ENDOR spectra were recorded using a Bruker ELEXSYS E500 spectrometer equipped with an Oxford CF935 cryostat. The ENDOR spectra were recorded at $T=6$ K with the microwave power ranging between 1 and 40 mW and the rf power ranging from 60 to 200 W.

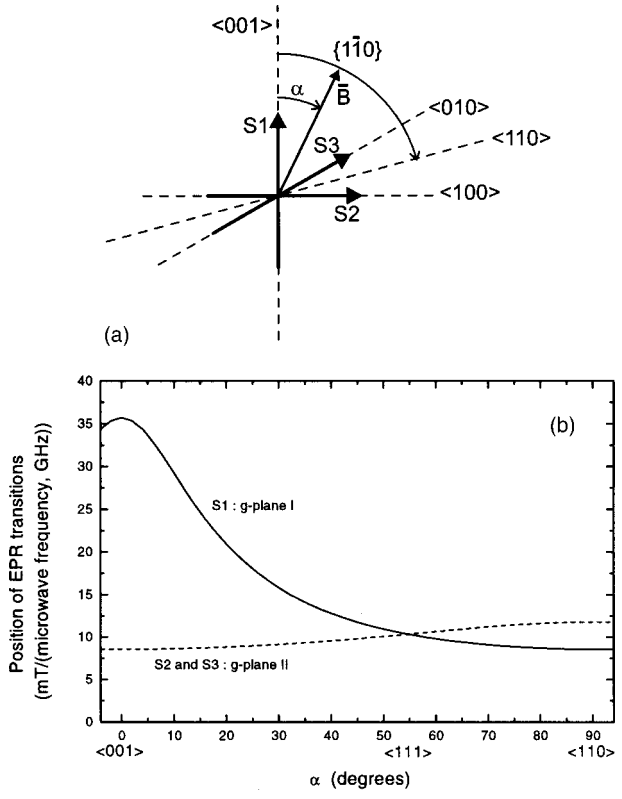

FIG. 1. (a) Three possible orientations of the tetragonal axis of the Fe^+(I) center in the cubic lattice of $SrCl_2$ indicated with arrows (*S*1, *S*2, and *S*3). (b) Angular variation of the low field EPR transitions ($M_S=\frac{1}{2}\leftrightarrow M_S=-\frac{1}{2}$) of the Fe^+(I) center in a {110} plane. The positions of the EPR transitions, as resulting from microwave *X*-band (9.56 GHz) and *Q*-band (34.00 GHz) measurements, are given in units of magnetic field over microwave frequency.

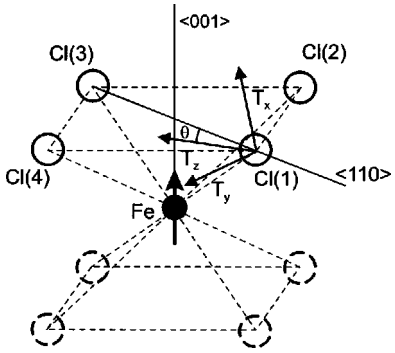

FIG. 2. Model used in the analysis of ENDOR spectra, consisting of a central Fe^+ ion, interacting with four equivalent neighboring Cl^- ions (full lines), labeled Cl(1)–Cl(4). The principal axes and principal values T_x, T_y, and T_z of an interaction tensor $\vec{T}$, are indicated in the figure. The principal direction corresponding to T_y is along a $\langle 1\bar{1}0\rangle$ axis. The principal directions corresponding to T_x and T_z are tilted away from ⟨001⟩ and ⟨110⟩, respectively, by an angle θ. The other four equivalent Cl^- ions in the first shell of neighbors are presented with interrupted lines.

III. RESULTS

A. Definition of *g* planes

$SrCl_2$ has the CaF_2 lattice structure with cubic symmetry (O_h^5 with $a=0.6977$ nm). The Fe^+(I) center has tetragonal symmetry.[3] If the magnetic field has an arbitrary direction with respect to the crystal axes, three magnetically inequivalent defect orientations can be observed [Fig. 1(a)]. For the magnetic field rotated in a crystal {110} plane two of these orientations, called *S*2 and *S*3 in Fig. 1(a), become magnetically equivalent. ENDOR spectra recorded with the magnetic field set to the EPR line position of these defect orientations will be denoted as being recorded in the *g* plane II. The other defect orientation [*S*1 in Fig. 1(a)] has its tetragonal axis in the {110} plane of rotation, called the *g* plane I. The corresponding low field EPR transitions ($M_S=\frac{1}{2}\leftrightarrow M_S=-\frac{1}{2}$) are presented in Fig. 1(b).

B. First shell Cl interactions

The interaction with only one shell of Cl nuclei could be identified in the ENDOR spectrum. The tetragonal symmetry of the *g* tensor implies that the Fe^+(I) center has either C_{4v} or D_{4h} symmetry. In the former case, the first shell contains four equivalent Cl nuclei, in the latter case eight, which are pairwise magnetically equivalent. As ENDOR does not give any direct information about the total number of interacting magnetically equivalent nuclei, it is unable to distinguish between these two cases. In discussing the ENDOR results an interaction with a shell of four Cl nuclei, represented in Fig. 2 with continuous lines, will be initially considered. The

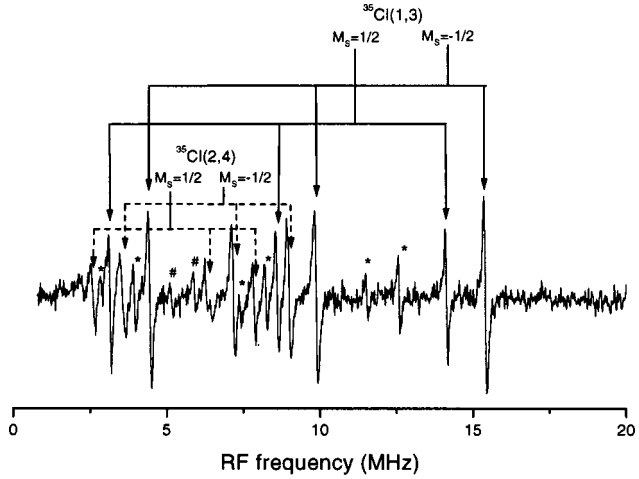

FIG. 3. *X*-band ENDOR spectrum (microwave frequency $\nu_{MW}=9.56$ GHz) with $B\|\langle 110\rangle$ in *g* plane I, recorded at 6 K. The transitions attributed to the shf interaction with the nuclei ^{35}Cl(1) and ^{35}Cl(3) are indicated with solid vertical lines. The corresponding ^{37}Cl transitions are indicated with an asterisk. The transitions assigned to the interaction with the second set of ^{35}Cl nuclei [Cl(2) and Cl(4)] are indicated with dashed vertical lines. The observed corresponding ^{37}Cl transitions are indicated with #.

other four Cl^{-} ligands forming the other comers of a cube are represented with interrupted lines.

1. ENDOR spectrum

Figure 3 presents the *X*-band ENDOR spectrum recorded in the range 0–20 MHz, with the magnetic field $B\|\langle 110\rangle$ in the *g* plane I ($g=g_{\perp}$). The observed resonances can be attributed to the interaction of the unpaired electrons with two magnetically inequivalent sets of Cl nuclei. One set corresponds to nuclei Cl(1) and Cl(3), the other consists of nuclei Cl(2) and Cl(4), with notations from Fig. 2. The interactions with the two Cl isotopes ^{35}Cl and ^{37}Cl (both with $I=\frac{3}{2}$) are observed in the expected intensity ratios for their natural abundance of 75.77 and 24.23 %, respectively.

Although the subset of EPR lines at which the ENDOR spectra were recorded [shown in Fig. 1(b)] can be formally described with an effective spin $S=\frac{1}{2}$, the ENDOR spectrum in Fig. 3 cannot be analyzed in this way. Indeed, for a center with an effective spin $S=\frac{1}{2}$ ($g_{\|}^{\mathrm{eff}}=g_{\|}$ and $g_{\perp}^{\mathrm{eff}}=2g_{\perp}$), interacting with a nucleus with $I=\frac{3}{2}$, six allowed ENDOR transitions ($\Delta M_S=0$, $\Delta M_I=1$) between the first order eigenvalues of the spin Hamiltonian (with usual notations[10]):

$$\hat{H}_s=\mu_B\mathbf{B}\cdot\vec{g}\cdot\hat{\mathbf{S}}+\hat{\mathbf{S}}\cdot\vec{A}\cdot\hat{\mathbf{I}}-g_N\mu_N\mathbf{B}\cdot\hat{\mathbf{I}}\cdot\vec{Q}\cdot\hat{\mathbf{I}} \tag{1}$$

should be observed at frequencies

$$h\nu_1=\frac{A}{2}+g_N\mu_N B+3Q,\quad h\nu_2=\frac{A}{2}+g_N\mu_N B,$$

$$h\nu_3=\frac{A}{2}+g_N\mu_N B-3Q,$$

$$h\nu_4=\frac{A}{2}-g_N\mu_N B+3Q,\quad h\nu_5=\frac{A}{2}-g_N\mu_N B,$$

$$h\nu_6=\frac{A}{2}-g_N\mu_N B-3Q. \tag{2}$$

Thus, two triplets of ENDOR transitions would be observed for each set of Cl nuclei and each isotope. The splitting between these triplets is $2g_N\mu_N B$. In the spectrum shown in Fig. 3 the two triplets of the ^{35}Cl isotope for set one are indicated. The splitting between them, however, is close to $4g_N\mu_N B$. This is confirming the previous analysis of the complete *X* band EPR spectrum[3] performed with a spin Hamiltonian with spin $S=\frac{3}{2}$. Consequently, the analysis of the interaction of the unpaired electrons with the magnetic Cl nuclei, has been performed with the following axial spin Hamiltonian (neglecting all interactions between the nuclei):

$$\hat{H}_S=\mu_B(g_{\|}B_z\hat{S}_z+g_{\perp}(B_x\hat{S}_x+B_y\hat{S}_y))+D\left(\hat{S}_z^2-\frac{1}{3}\hat{S}^2\right)$$
$$+\hat{\mathbf{S}}\cdot\vec{A}\cdot\hat{\mathbf{I}}-g_N\mu_N\mathbf{B}\cdot\hat{\mathbf{I}}+\hat{\mathbf{I}}\cdot\vec{Q}\cdot\hat{\mathbf{I}}, \tag{3}$$

where the first two terms in the above formula describe the EPR spectra with parameters[3] $g_{\|}=2.000$, $g_{\perp}=4.175$, and $D=121.5$ GHz. Assuming that the principal axes of the superhyperfine (shf) **A** and quadrupole **Q** tensors coincide with those of the **g** tensor, the ENDOR transitions with the magnetic field perpendicular to the tetragonal axis of the center ($B_z=0$) can be calculated to first order to occur at

$$A^{*}\pm g_N^{*}\mu_N B\begin{cases}+3Q,\\ +0,\\ -3Q,\end{cases}$$

with

$$A^{*}=A\left[1-\frac{3}{4}\left(\frac{h\nu_{mw}}{2D}\right)^2\right]\ \text{and}\ g_N^{*}=g_N\left(1+\frac{3}{4}\frac{g_{\perp}\mu_B A}{g_N\mu_N D}\right). \tag{4}$$

Because the *X*-band microwave quantum ($h\nu_{mw}$) is about ten times smaller than the zero field splitting parameter *D*, the center of the two triplets can be taken as a first order estimate for the shf interaction parameter *A*. Using the above mentioned EPR parameters, the splitting between the triplets is found to be $3.8g_N\mu_N B$, in very close agreement with the observed value.

2. ENDOR angular variation

The angular variation of the ENDOR spectrum has been recorded in both *g* planes, in the two microwave frequency bands. The *X*- and *Q*-band ENDOR angular variations in *g* plane I for the ^{35}Cl sotope are shown in Fig. 4, along with simulations using the spin Hamiltonian parameters given in Table I. The resonance frequencies were calculated by diagonalization of the spin Hamiltonian (3). The ENDOR parameters in Table I were obtained by least square error fitting the *X*-band data in both *g* planes. The intensity and line width of

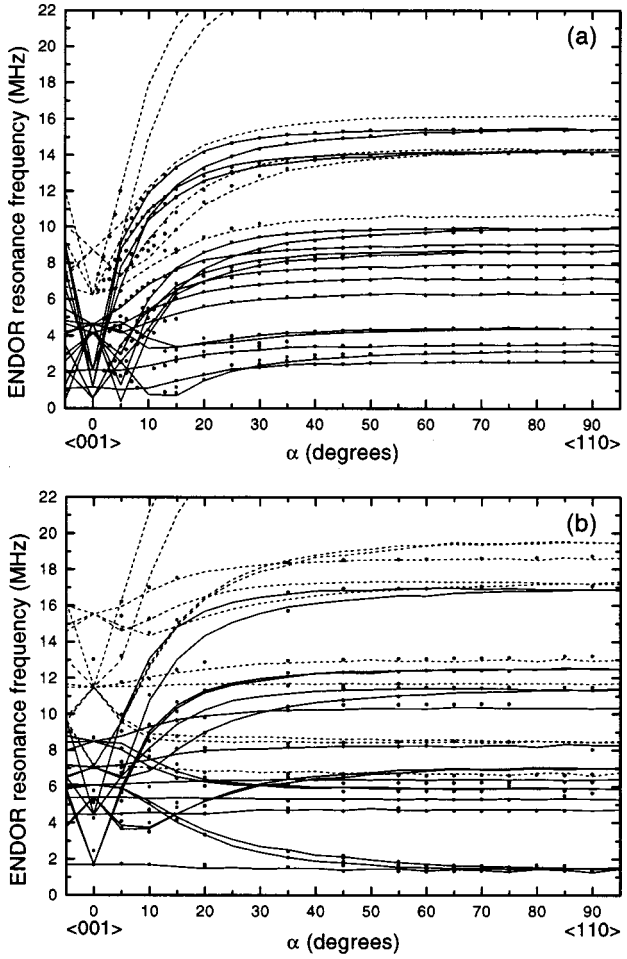

FIG. 4. Angular variation of the ^{35}Cl ENDOR spectrum in g plane I in the (a) X band ($\nu_{MW}=9.56$ GHz) and (b) Q band ($\nu_{MW}=34.00$ GHz), recorded at 6 K. The experimental data are represented by filled circles. Simulated angular variation, calculated with the ENDOR data in Table I, is shown for the allowed ($\Delta M_I=1$, full lines) and forbidden ($\Delta M_I=2$, dashed lines) transitions.

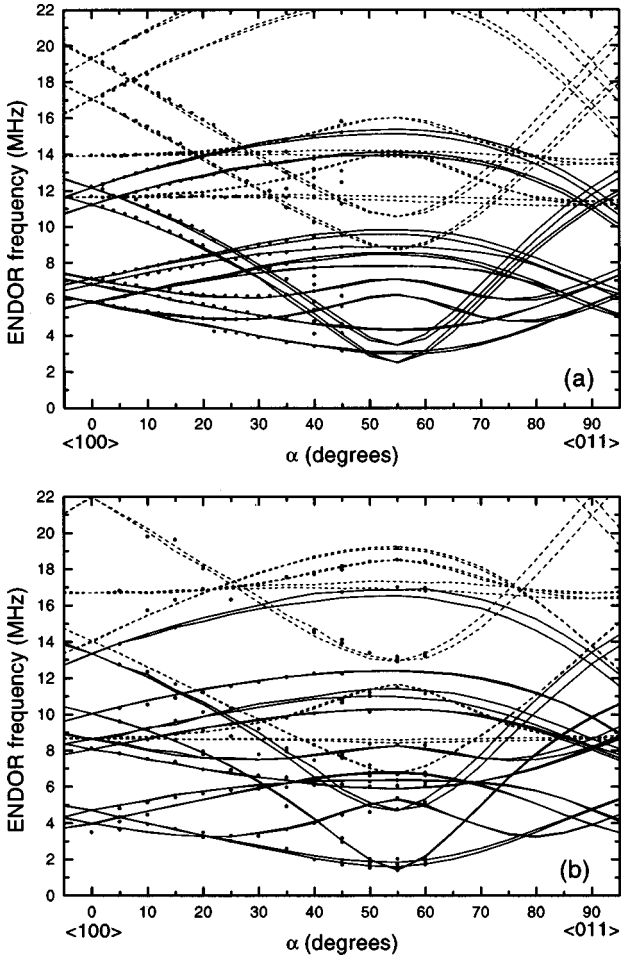

FIG. 5. Angular variation of the ^{35}Cl ENDOR spectrum in g plane II in (a) the X band ($\nu_{MW}=9.56$ GHz) and (b) Q band ($\nu_{MW}=34.00$ GHz), recorded at 6 K. The experimental data points are represented by filled circles. Simulated angular variation, calculated with the ENDOR data in Table I, is shown for the allowed ($\Delta M_I=1$, full lines) and forbidden ($\Delta M_I=2$, dashed lines) transitions.

TABLE I. Spin Hamiltonian parameters of the Fe^+(I) center in $SrCl_2$, including the EPR parameters, as reported in Ref. 3. The zero field splitting parameter D, the shf and quadrupole principal values are given in MHz. The principal axes of the Cl interaction tensors are defined in Fig. 2. The angles are given in degrees. The principal axes of the ^{57}Fe interaction are coincident with the principal g axes. The errors in the last digits are given as a subscript.

EPR parameters								
$g_\parallel$		$g_\perp$			D			
2.000_g		4.175_3			121500_{500}			
ENDOR parameters								
^{35}Cl	A_x	A_y	A_z	θ_A	Q_x	Q_y	Q_z	θ_Q
	2.55_{10}	5.78_3	9.37_3	7_1	$\pm 0.86_3$	$\pm 0.98_2$	$\mp 1.84_2$	7_1
^{57}Fe	$^{57}A_\parallel$	$^{57}A_\perp$						
	-31.2_3	-41.0_5						

the ENDOR transitions strongly depend on the orientation of the magnetic field, especially in the Q band.

The symmetry of the center requires that one of the principal axes of the A and Q interaction tensors is along a crystal $\langle 1\bar{1}0\rangle$ direction, indicated as the y axis in Fig. 2. The other two axes x and z may be tilted away from $\langle 001\rangle$ and $\langle 110\rangle$ respectively, by an angle θ. If $\theta \neq 0$, the nuclei Cl(1) and Cl(3) become magnetically inequivalent when the magnetic field is rotated away from the $\langle 110\rangle$ direction (90°) in g plane I. This is indeed observed in the angular dependence, as a splitting of the corresponding transitions. Meanwhile, the nuclei Cl(2) and Cl(4) remain magnetically equivalent. No splitting is observed for these lines. When the magnetic field is directed along $\langle 001\rangle$ (0°), all four chlorine nuclei are magnetically equivalent and the corresponding transitions coincide.

Figures 5(a) and 5(b) present the X- and Q-band angular variation of the ^{35}Cl ENDOR spectrum in g plane II, respectively. The corresponding transitions could only be followed

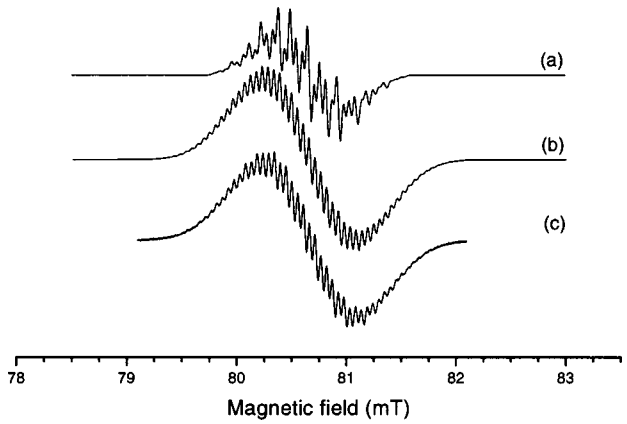

FIG. 6. EPR spectrum with $B\|\langle 100\rangle$ in g plane II at $\nu_{MW}=9.44$ GHz. Simulated shf interaction with (a) four equivalent $^{35}Cl/^{37}Cl$ nuclei, (b) eight equivalent $^{35}Cl/^{37}Cl$ nuclei, and (c) experimental spectrum recorded at 10 K with low (0.01 mT) modulation amplitude.

over a limited angular range, as their intensity dropped drastically when the magnetic field was rotated towards the $\langle 011\rangle$ direction. In an arbitrary direction in this plane, all four Cl nuclei are magnetically inequivalent. As the angle θ is small (7°) the inequivalence between Cl(1) and Cl(3) and between Cl(2) and Cl(4) is very subtle. The corresponding splitting of the observed transitions is barely resolved in the recorded angular range. The observation of ENDOR forbidden transitions ($\Delta M_S=0, \Delta M_I=2$) in this g plane, especially in the X band, has facilitated the analysis of the spectra.

Examining the ^{35}Cl ENDOR spin Hamiltonian parameters presented in Table I, the following points should be noted: the principal axes of the **A** and **Q** tensors coincide within experimental error. The largest shf and quadrupole tensors principal values are found along the direction pointing towards the central Fe nucleus. However, this principal direction largely deviates (with 28°) from the Fe-Cl bond axis, which is at 35°16′ for a Fe ion situated in the center of a cube of Cl ions. ENDOR does not allow determining the absolute signs of the principal shf and quadrupole tensor components. It could, however, be determined that all principal hyperfine tensor components have the same sign, which we assume to be positive. The relative signs of the quadrupole values with respect to that of the shf values could not be determined.

3. Superhyperfine structure in the EPR spectrum

As mentioned in the Introduction to this section, ENDOR gives no information concerning the total number of equivalent Cl nuclei in this case and leaves unanswered the question whether the first shell contains four or eight Cl^- ions. In the X-band EPR spectrum, with $B\|\langle 100\rangle$ in g plane II, a partially resolved complex shf pattern has been observed [Fig. 6(c)]. The experimental spectrum was recorded with a modulation amplitude of 0.01 mT, after carefully orienting the crystal with the aid of the EPR transitions of the Fe_t^{3+} center.

The simulation of the EPR spectrum using the ENDOR data allows the determination of the number of equivalent interacting nuclei. The result of such simulations is presented in Figs. 6(a) and 6(b) assuming an interaction with four and eight equivalent Cl nuclei, respectively. In the former case, the interaction with the other set of four Cl nuclei (indicated in dashed lines in Fig. 2) is assumed to be very small, because it has not been detected in the ENDOR spectrum. It should thus only contribute to the line width of the individual shf EPR transitions. The simulated spectra were calculated by considering both allowed ($\Delta M_S=1$ and $\Delta M_I=0$) and forbidden ($\Delta M_S=1$ and $\Delta M_I: \pm\frac{3}{2}\leftrightarrow\pm\frac{1}{2}$) EPR transitions and assuming that each additional interacting nucleus splits each shf line in the same way. Contributions of all possible conformations of ^{35}Cl and ^{37}Cl nuclei were added in ratios according to their statistical probability. Comparing the simulated and observed spectra, it is clear that four equivalent Cl nuclei cannot reproduce the observed shf pattern. On the contrary, the spectrum calculated with eight equivalent Cl nuclei is in excellent agreement with the observed spectrum. The best agreement between experimental and simulated spectra was obtained assuming that the individual shf lines exhibit a Gaussian shape and a line width of 0.048 mT. The fact that all 8 Cl^- ligands are equivalent implies that the center has D_{4h} symmetry.

The $g_\|$ component of the EPR spectrum also exhibits a partially resolved shf structure. However, in freshly irradiated crystals, containing the Fe_t^{3+} center, used for orienting the crystal, the $g_\|$ spectrum of $Fe^+(I)$ overlaps the spectra of the other paramagnetic Fe^+ and Fe^{3+} centers. Annealed crystals, on the other hand, could not be equally well oriented. For these reasons, we did not simulate the shf structure for this defect orientation.

C. Hyperfine interaction with the central ^{57}Fe nucleus

In addition to, and well separated from the Cl transitions, two transitions with lower intensity were observed in the X-band ENDOR spectra, in the frequency range 10–45 MHz. These transitions could not be detected in the Q-band ENDOR spectrum, most probably due to the overall lower signal intensity as compared with the X-band spectra. Their angular dependence, shown in Fig. 7, suggests an interaction of the unpaired electrons with a nucleus located on the tetragonal axis of the center. For each magnetic field orientation, only two transitions are observed. At $g_\perp$ the splitting between the lines is about twice as large as at $g_\|$. The lines cross when the magnetic field is rotated about 5° away from $\langle 001\rangle$ in g plane I. It was checked with electron nuclear triple resonance that these transitions belong to different M_S states. Although the hyperfine coupling corresponding to this interaction is much larger than that of the interaction from the first chlorine shell, it cannot be observed in the EPR spectrum (the complete spectrum can be reproduced without taking it into account). This fact indicates that the corresponding nucleus has a very low natural abundance. For an iron-related center in $SrCl_2$, $^{57}Fe\,(2.15\%, I=\frac{1}{2}, g_N=0.1806)$ and $^{87}Sr\,(7.0\%, I=\frac{9}{2}, g_N=-0.24291)$ are the most obvious candidates. As only two transitions are observed for each magnetic field orientation, we assign these transitions to the hyperfine interaction with the central ^{57}Fe nucleus. A good

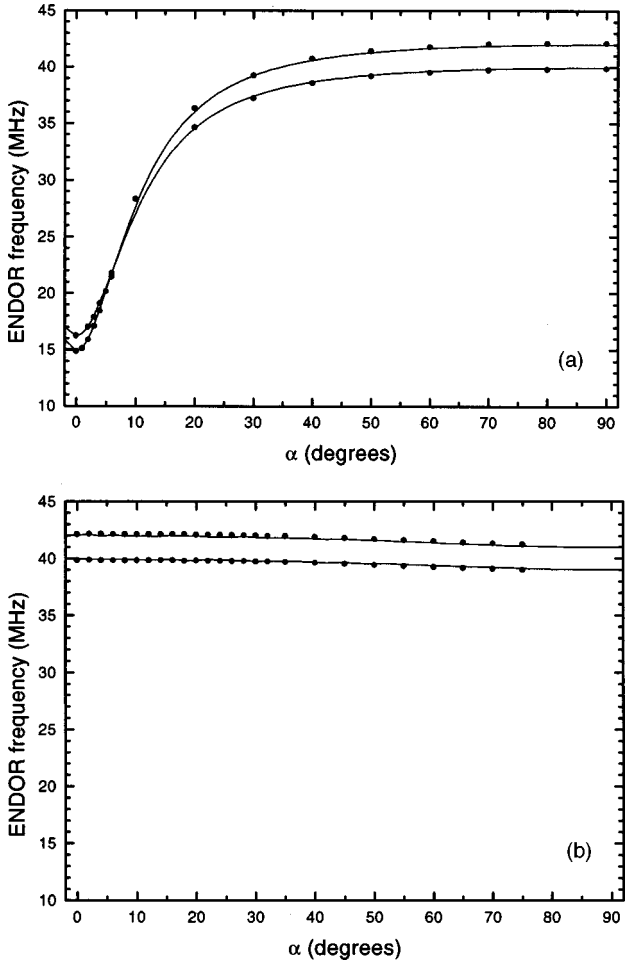

FIG. 7. *X*-band ($\nu_{MW}=9.56$ GHz) angular variation of the ^{57}Fe ENDOR spectrum in *g* plane I (a) and *g* plane II (b), recorded at 6 K. Experimental data (full circles) and simulated angular dependence (continuous line).

fitting of the angular dependence of these transitions could only be obtained by assuming that the hyperfine values are negative (principal values given in Table I). The crossing of the transitions can then be explained as follows. For each magnetic field orientation, the ENDOR frequencies are given by

$$|A^{\text{eff}}M_S - g_N^{\text{eff}}\mu_N B|. \tag{5}$$

At $g_\parallel$, the levels between which the EPR transition occurs are pure $M_S=\pm\frac{1}{2}$ states for which $A^{\text{eff}}=A_\parallel$ and $g_N^{\text{eff}}=g_N$. If $A_\parallel<0$, the $M_S=-\frac{1}{2}$ transition occurs at a lower frequency than the $M_S=\frac{1}{2}$ transition. At $g_\perp$, $A^{\text{eff}}\approx 2A_\perp$ and $g_N^{\text{eff}}=g_N^*$ [see Eq. (4)]. As the latter value is negative for negative $A_\perp$, the $M_S=-\frac{1}{2}$ transition will now occur at the highest transition frequency. If the magnetic field is rotated in the *g* plane I, from $g_\parallel$ to $g_\perp$, the ENDOR lines should thus cross.

From the best fit hyperfine parameters in Table I, the hyperfine splitting in the EPR spectrum can be calculated to be $^{57}A_\parallel=-1.1$ mT and $^{57}A_\perp=-0.7$ mT. These hyperfine values are very similar to the ones observed for the Fe^+ center in ThO_2 ($^{57}A_\parallel=1.19$ mT and $^{57}A_\perp=0.88$ mT, signs not determined), which strongly supports the present analysis, based on the expected similar core polarization fields in the two cases.[9]

It should be mentioned that an equally good fitting of the angular dependence for these transitions may be obtained by assuming that the interacting nucleus is ^{87}Sr and taking the *A* values positive. However, for a ^{87}Sr nucleus, two M_S multiplets of nine ENDOR transitions, split by the nuclear quadrupole interaction, are expected for each magnetic field orientation. In spite of a careful search, no evidence for such quadrupole splitting of the transitions has been observed. Moreover, it is not easy to explain why the hyperfine values for an interaction with a ^{87}Sr nucleus on the tetragonal axis of the complex should be so large and strongly anisotropic. Indeed, as the unpaired electrons for an ion in the $^4\Gamma_8$ ground state are mainly localized in d_{xy}, d_{yz}, and d_{zx} orbitals, there is no direct overlap with the orbitals of the ligands on the *z* axis of the complex. Therefore, we consider the possibility of assigning the transitions to ^{87}Sr improbable. Conclusive evidence for the assignation of the interaction to the central nucleus could be obtained from experiments on crystals doped with ^{57}Fe isotopically enriched iron.

IV. STRUCTURAL MODELS OF THE Fe^+(I) CENTER AND ITS PRECURSOR

Our primary objective is to propose a microscopic model for the center under study. As the Fe^+(I) center is produced at 80 K without additional thermal anneal, it may be assumed that it has the same structure as its precursor Fe^{2+}(I) center, except for a possible relaxation of the surrounding lattice following the electron trapping. Moreover, considering the short irradiation times in which a large amount of Fe^+(I) centers are produced at low temperature, it is highly unlikely that the production or migration of vacancies or interstitials play a role in its formation. Consequently, the structural models to be further on discussed shall refer to both Fe^+(I) center and its Fe^{2+}(I) precursor.

No additional information could be obtained from pulse annealing experiments, because the center itself does not decay and it is not formed through the decay of other paramagnetic centers. The ENDOR data do not provide enough information to propose an exclusive model, but offer the basis for ruling out the majority of the simplest models presented in Fig. 8.

A. Position of the central Fe ion

The $SrCl_2$ lattice consists of cubic cells cornered by eight Cl^- ions alternatively filled with a Sr^{2+} ion or empty [see, e.g., Fig. 8(a)]. The Fe^+ ion can be either in a Sr^{2+} position (substitutional) or reside in an empty cell (interstitial). The coordination by eight Cl^- ions is in both cases the same. However, in the former case the neighboring cells are empty whereas in the latter they are occupied with a Sr^{2+} ion. Thus, the position of the Fe^+ ion in the lattice can only be identified in an unambiguous way through the observation of the nearest shell of Sr^{2+} ions. Unfortunately, we have observed no convincing evidence for interactions of that kind. This

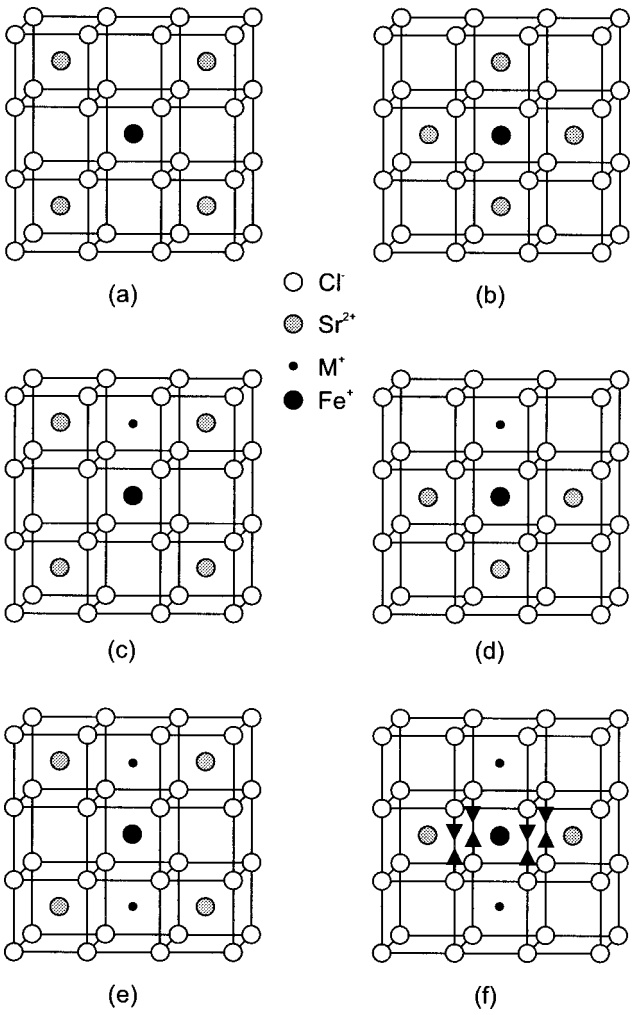

FIG. 8. Simplest models of the Fe^+(I) center in $SrCl_2$:Fe^{2+} single crystals grown in a chlorine atmosphere. (a) Substitutional, isolated Fe^+ ion. (b) Interstitial isolated Fe^+ ion. (c) Substitutional model with a nearby interstitial cation impurity. (d) Interstitial model with a nearby substitutional cation impurity. (e) Substitutional Fe^+ with two nearby cation impurities on the [001] axis. (f) Interstitial Fe^+ with two nearest substitutional cation impurities on the [001] axis. The tetragonal compression of the first shell of Cl^- ligands is indicated by arrows.

may be due to the low natural abundance of the magnetic ^{87}Sr isotope. Moreover, this isotope has a low nuclear magnetic moment and a high nuclear spin ($I=\frac{9}{2}$). The former fact implies that interactions with ^{87}Sr nuclei are expected at low rf frequencies (possibly below the detection limit of the spectrometer 0.8 MHz) and the latter implies that each interaction gives rise to a set of 18 ENDOR transitions, further decreasing the intensity of an individual ENDOR resonance. Because Fe^{2+} has the same valence state as the cations in $SrCl_2$, it is expected to occupy substitutional positions. However, the presence of interstitial Fe^{2+} in the structurally similar CaF_2 lattice has been suggested by Sato based on Mössbauer spectroscopy results.[11] Both substitutional and interstitial models are in agreement with our ENDOR results and will be considered here.

B. Isolated Fe^+ models

The simplest models for Fe^+(I) would be an electron trapped at a substitutional [Fig. 8(a)] or at an interstitial Fe^{2+} ion [Fig. 8(b)]. The substitutional model immediately leads to a problem. The isolated substitutional Fe^{2+} ion acts as a hole trap in $SrCl_2$ single crystals, grown in vacuum or in an inert atmosphere, giving rise to the cubic Fe_c^{3+} center upon irradiation at low temperature.[4] If this Fe^{2+} ion would also be the precursor of the Fe^+(I) center, it should also be produced in crystals grown in this way. Because of its net charge of $+2e$,Fe^{2+} in an interstitial position is expected to act as a deep electron trap rather than a hole trap. However the model in Fig. 8(b) cannot explain the strong tetragonal distortion of the Fe^+(I) center (g anisotropy, D term, axially compressed first shell Cl^- ions). Indeed, eightfold coordinated Fe^+ has an orbital singlet ground state ($^4\Gamma_8$) and is not expected to exhibit a Jahn-Teller distortion. EPR results on the isoelectronic eightfold coordinated Co^{2+} in $SrCl_2$, e.g., show that this center has undistorted cubic symmetry.[12] It may thus be concluded that the axial symmetry of the center is due to the presence of other defects in the neighborhood of the Fe^+ ion.

C. Fe^+-M^+ pairs (M=Na or K)

In previous EPR studies[2,3] the strong **g** tensor anisotropy and the large zero field splitting have been attributed to an interstitial M^+ impurity next to the substitutional Fe^+ ion. The corresponding model is shown in Fig. 8(c) and for the sake of symmetry in the discussion, we shall also consider the case of M^+ being in the substitutional position while Fe^+ is interstitial [Fig. 8(d)]. The cation impurities were proposed to be Na^+ or K^+, as these ions are known to be the dominant unintentional impurities in $SrCl_2$ with concentrations (below 100 ppm) comparable to that of the Fe^+(I) centers. Although such models perfectly explain the stability of the center (it is electrically neutral) and the fact that the precursor acts as a deep electron trap (it has a net charge of $+e$), they have to be rejected because they have C_{4v} symmetry, whereas the present EPR and ENDOR results demonstrate that the Fe^+(I) center has D_{4h} symmetry.

D. $M^+-Fe^+-M^+$ models

Models which have D_{4h} symmetry can be derived from the structures presented in Figs. 8(c) and 8(d) by adding an identical cation on the tetragonal axis of the center in such a way that it acquires inversion symmetry. These models are shown in Figs. 8(e) and 8(f) for substitutional and interstitial Fe^+, respectively. The presence of the cation impurities may explain the strongly axial character of the Fe^+(I) center. However, it has to be kept in mind that these impurities are present in the crystals in fairly low concentrations.

In the case of substitutional Fe^+, no driving force seems to be keeping the M^+ ions bound to the complex. The concentration of the precursor center is expected to be dominated by the statistical probability of two of these ions and one Fe^{2+} ion being arranged in this way in the crystal, which appears to be very low. As the concentration of Fe^+(I) cen-

ters appears to have the same order of magnitude as that of other paramagnetic Fe centers, e.g., the Fe_c^{3+} centers, the model presented in Fig. 8(e) seems rather unlikely.

In the case of interstitial Fe^+, the presence of two substitutional M^+ ions is required for the charge compensation of the precursor, which is then electrically neutral. Although the statistical probability of finding such an arrangement of ions is low, the charge compensation mechanism would make it energetically favorable. The model in Fig. 8(f) does not explain *a priori* the high stability of the Fe^+(l) center, though, as it would have a net charge of $-e$. The charge compensation may, however, be preserved by the presence of a remote positively charged defect such as an interstitial cation or a Cl^- vacancy.

Related to this model the remaining questions are what is the nature of the impurity ions and why have they not been observed in the ENDOR spectra? In the reconstruction of the $g_\perp$ EPR spectrum from the chlorine ENDOR data, a residual linewidth of 0.048 mT was observed. If the impurity ions are assumed to be either Na^+ or K^+, this line width may be explained by an unresolved shf pattern of two equivalent nuclei with $I=\frac{3}{2}$ (seven line pattern with intensity ratios 1:2:3:4:3:2:1). This limits the shf parameter $A_\perp$ to about 1 MHz. As the ions are situated on the axis of the center, the $A_\parallel$ value is expected to be larger. In the case of ^{23}Na ($g_N=1.477$) the Larmor frequency ranges from 0.92 MHz at $g_\perp$ to 3.85 MHz at $g_\parallel$ in the *X*-band microwave frequencies and from 3.27 MHz to 13.63 MHz in the *Q* band. Because these values, especially in the *Q* band and in the $g_\parallel$ region, are well above the detection limit of our ENDOR spectrometers, the corresponding transitions should have been observed. We therefore reject the possibility of Na^+ impurities. The nuclear magnetic moment of ^{39}K is much smaller ($g_N=0.261$). In the *X* band the Larmor frequency does not exceed 0.7 MHz and even in the *Q* band it remains below 2.5 MHz. It is thus possible that a weak interaction with two equivalent K^+ ions remained undetected in the ENDOR spectra.

E. Models involving more than one Fe ion

In view of the high iron concentration in the crystals ($\sim$300 ppm), aggregates of Fe^{2+} ions, such as dimers and trimers, may be incorporated in the crystals during growth. After irradiation at 80 K, such defects may trap electrons and become EPR active. Because both $Fe^{2+}(S=1)$ and $Fe^+(S=\frac{3}{2})$ are paramagnetic ions, such centers should be treated as coupled spin systems. In order to be a possible model for the Fe^+(I) center, the resulting system should have a half integer electron spin with a value of at least $\frac{3}{2}$. Indeed, considering the spin Hamiltonian (3) in which the zero field splitting is much larger than the electronic Zeeman energy, there will only be a first order contribution of the $M_s=\pm\frac{3}{2}$ levels to the ground state doublet $M_s=\pm\frac{1}{2}$ and the EPR and ENDOR characteristics of the center may be described quite accurately using an effective spin $S=\frac{3}{2}$. A possible model for the Fe^+(I) center should, of course, still have D_{4h} symmetry (e.g., a pair of Fe interstitials along a $\langle 100\rangle$ axis with a Sr^{2+} vacancy in between would have the right symmetry).

As the ^{57}Fe isotope has very low natural abundance, no information about the number of interacting Fe nuclei can be obtained from the EPR spectrum. Moreover, possible weaker interactions with other ^{57}Fe nuclei may easily be obscured by the more intense first shell Cl ENDOR spectrum. In order to examine this possibility, additional experiments on ^{57}Fe enriched $SrCl_2$:Fe^{2+} crystals are required.

V. CONCLUSIONS

The Fe^+(I) center, produced after x or γ ray irradiation at liquid nitrogen temperature of chlorinated $SrCl_2$:Fe^{2+} single crystals, has been studied with *X*- and *Q*-band ENDOR. Interactions of the unpaired electrons with the first shell of Cl nuclei and with the central ^{57}Fe nucleus have been identified in the ENDOR spectra. The reconstruction of the *X*-band EPR spectrum using the ENDOR data showed that all eight Cl^- ions in the first shell are equivalent. Hence the center has D_{4h} symmetry. Moreover, the ENDOR data strongly suggest that the first shell of Cl^- ions exhibits a tetragonal compression. The simplest structural model which can explain all experimental data consists of an interstitial Fe^+ ion with two neighboring substitutional cation impurities, most likely K^+, on opposite sites along the tetragonal axis of the center. The unusually high stability of the resulting Fe^+ center can only be explained by considering the additional presence of positively charged defects in the crystal, and/or by an energetically favorable, strong relaxation of the neighboring lattice following the electron trapping at the Fe^{2+}(I) precursor center. However, a model consisting of a dimer or trimer of Fe^{2+} ions as precursor center cannot be completely ruled out.

ACKNOWLEDGMENTS

This work was performed under the auspices of a Flemish-Romanian collaborative scientific research project (BIL96/57) and partially supported by ANSTI Grant No. B4/1999. The Fund for Scientific Research–Flanders (Belgium) is acknowledged for financial support.

[1] S. V. Nistor, D. P. Lazar, H. Kaess, and D. Schoemaker, Solid State Commun. **104**, 521 (1997).

[2] S. V. Nistor and D. Schoemaker, Rom. J. Phys. **43**, 131 (1998).

[3] S. V. Nistor, M. Stefan and D. Schoemaker, Phys. Status Solidi B **214**, 229 (1999).

[4] J. M. De Siebenthal, D. Nicollin, and H. Bill, Chem. Phys. Lett. **58**, 317 (1978).

[5] Th. Pawlik, S. V. Nistor, and J. M. Spaeth, J. Phys.: Condens. Matter **9**, 7631 (1997), and references therein.

[6] E. Boesman, F. Callens, J. Haes, F. Maes, P. Matthys, and P. Moens, Solid State Commun. **77**, 931 (1991).

[7] F. J. Callens, F. Maes, P. Matthys, P. Moens, and E. Boesman,

Phys. Status Solidi B **170**, 609 (1992).
[8] W. Gehlhoff and W. Ulrici, Phys. Status Solidi B **102**, 11 (1980).
[9] S. A. Marshall and S. V. Nistor, Phys. Rev. B **6**, 24 (1973).
[10] J. R. Pilbrow, *Transition Ion Electron Paramagnetic Resonance* (Clarendon Press, Oxford, 1990).
[11] Y. Sato, Phys. Status Solidi B **82**, 611 (1977).
[12] K. E. Roelfsema and H. W. den Hartog, J. Magn. Reson. **29**, 255 (1978).